ACS Catalysis

Research Article

pubs.acs.org/acscatalysis

Investigating the Influence of Mesoporosity in Zeolite Beta on Its Catalytic Performance for the Conversion of Methanol to Hydrocarbons

Zhaohui Liu,[†] Xinglong Dong,[†] Yihan Zhu,[†] Abdul-Hamid Emwas,[‡] Daliang Zhang,[‡] Qiwei Tian,[†] and Yu Han*[,†]

[†]Advanced Membranes and Porous Materials Center, Physical Sciences and Engineering Division, and [‡]Imaging and Characterization Core Lab, King Abdullah University of Science and Technology, Thuwal 23955-6900, Saudi Arabia

Supporting Information

ABSTRACT: Hierarchically porous zeolite Beta (Beta-MS) synthesized by a soft-templating method contains remarkable intracrystalline mesoporosity, which reduces the diffusion length in zeolite channels down to several nanometers and alters the distribution of Al among distinct crystallographic sites. When it was used as a catalyst for the conversion of methanol to hydrocarbons (MTH) at 330 °C, Beta-MS exhibited a 2.7-fold larger conversion capacity, a 2.0-fold faster reaction rate, and a remarkably longer lifetime in comparison to conventional zeolite beta (Beta-C). The superior catalytic performance of Beta-MS is attributed to its hierarchical structure, which offers full accessibility to all catalytically active sites. In contrast, Beta-C was easily deactivated because a layer of coke quickly deposited on the outer surfaces of the catalyst crystals, impeding access to interior active sites. This difference is clearly demonstrated by using electron microscopy combined with electron energy loss spectroscopy to probe the distribution of coke in the deactivated catalysts. At both low and high conversions, ranging from 20% to 100%, Beta-MS gave higher selectivity toward higher aliphatics (C_4−C_7) but lower ethene selectivity in comparison to Beta-C. Therefore, we conclude that a hierarchical structure decreases the residence time of methylbenzenes in zeolite micropores, disfavoring the propagation of the aromatic-based catalytic cycle. This conclusion is consistent with a recent report on ZSM-5 and is also strongly supported by our analysis of soluble coke species residing in the catalysts. Moreover, we identified an oxygen-containing compound, 4-methylbenzaldehyde, in the coke, which has not been observed in the MTH reaction before.

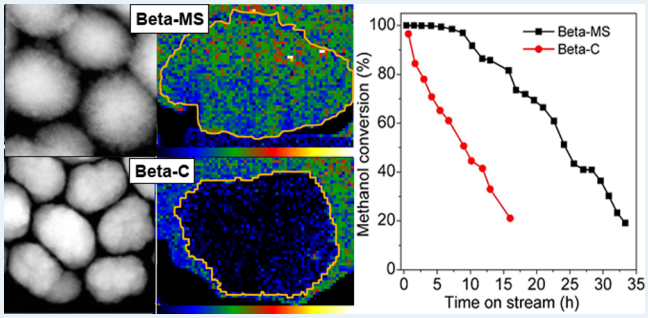

KEYWORDS: *hierarchical zeolite, methanol to hydrocarbons, electron energy loss spectroscopy, dual-cycle mechanism, coke formation*

INTRODUCTION

Zeolites are microporous aluminosilicates with regular intracrystalline cavities and channels of molecular dimensions. The small pore sizes of zeolites (0.3—1 nm) render unique size and shape selectivity in catalysis[1,2] but give rise to constraints for molecular diffusion within zeolite crystals.[3] As a consequence, zeolite-catalyzed reactions are often limited by slow diffusion. Decreasing the size of zeolite crystals could reduce the diffusion length, but this method is not favorable because it is difficult to synthesize zeolite crystals smaller than 100 nm, and furthermore, ultrafine catalyst particles are difficult to handle and are thus undesirable for practical applications.[4,5] An alternative and perhaps more effective method to circumvent the diffusion limitation imposed by small pores is to create a large number of mesopores (>2 nm) in zeolite crystals.[6−8] With this strategy, it is possible to significantly reduce the diffusion length (down to several nanometers), because mesopores break the microporous zeolitic framework into small domains. The resulting materials are usually referred to as "hierarchical zeolites" or "mesoporous zeolites," in which mesopores allow rapid diffusion and enhanced accessibility for bulky molecules, while zeolitic micropores enable catalytic activity and selectivity.[9−11]

Conventional methods for preparing hierarchical zeolites are based on various postsynthesis processes such as steaming,[12] acid (or base) leaching,[13,14] and chemical treatments.[15−17] Recently, more efforts have been made toward the "direct synthesis" of hierarchical zeolites through soft-templating routes,[18−21] which can achieve greater mesoporosity, more precise control of pore size, and higher zeolite structure integrity in comparison with "post-treatment" methods. Hierarchical zeolites prepared by different methods have been tested as catalysts for various reactions, and typically, they exhibit higher catalytic activities (especially when the reactant

Received: June 26, 2015
Revised: August 24, 2015
Published: August 26, 2015

DOI: 10.1021/acscatal.5b01350
ACS Catal. 2015, 5, 5837−5845

molecules are bulky),[22,23] longer lifetimes,[24,25] slower coke formation rates,[26] and altered product selectivities[27] in comparison to conventional zeolites with the same framework types. For example, we recently reported that a nonsurfactant cationic polymer can act as a dual template to synthesize hierarchical zeolite Beta.[28] The obtained material (Beta-MS) featured remarkable mesoporosity, single crystallinity, excellent stability, and superior catalytic activity over conventional zeolite Beta in several liquid-phase reactions. Although there is a bulk of evidence for the superior catalytic properties of hierarchical zeolites, a systematic comparison between a hierarchical zeolite and its bulk (nonmesoporous) counterpart for a particular reaction on the basis of detailed catalyst characterization and a careful analysis of the full products is lacking.

The conversion of methanol to hydrocarbons (MTH) has attracted considerable attention in the past few decades, because it provides an alternative way to produce fuels and chemicals that are currently mainly produced by petroleum-based synthetic routes. Acidic zeolites are the most commonly used catalysts for MTH reactions.[29] It is generally accepted that MTH reactions on zeolites follow an indirect "hydrocarbon pool" mechanism,[30,31] in which the active intermediates repeatedly undergo methylation or cracking reactions to produce complex hydrocarbons, and that there are two catalytic cycles coexisting in the process: an aromatic-based cycle and an olefin-based cycle, in which polymethylbenzenes and olefins act as the active hydrocarbon pool species, respectively (Scheme 1).[32−34] This dual-cycle mechanism may explain the observed

Scheme 1. Proposed Dual-Cycle Mechanism for Methanol to Hydrocarbon Conversions over Zeolite Catalysts[a]

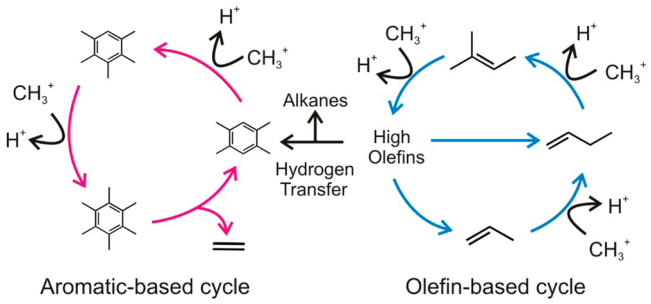

[a]Although this mechanism was proposed for the ZSM-5 systems,[30−32] it can also be used to explain the catalytic behaviors of other types of zeolites. The major intermediate species of the aromatic-based cycle (methylbenzenes) may differ in different zeolites due to pore size differences.

product selectivity of MTH on different zeolites by considering how the pore structure of the zeolite catalyst affects the relative propagation of the two cycles.[29] For example, ZSM-22 has one-dimensional noninteracting 10-membered-ring channels that are too small to form polymethylbenzene intermediates; consequently, the aromatic-based cycle is suppressed while the olefin-based cycle dominates the conversion process, giving rise to high selectivity for branched C_{5+}-fraction alkenes.[35,36] In contrast, SAPO-34 has large 12-membered-ring cavities with small (3.8 × 3.8 Å) pore openings that enrich aromatic intermediates, promoting the aromatic-based cycle to produce more ethene[37] (a termination product of this cycle; see Scheme 1). Likewise, the MTH product distribution over ZSM-5 can be tuned by varying the reaction conditions (e.g., feed compositions[38−40] and zeolite crystal sizes[4,41,42]) to adjust the relative propagation of these two catalytic cycles.

Hierarchical zeolites have been used for MTH, mainly based on the ZSM-5 system. Schmidt et al.[43] prepared hierarchical ZSM-5 zeolite via the desilication reassembly technique for MTH conversion. They found that, in addition to a longer lifetime, hierarchical ZSM-5 shows a deactivation/reactivation behavior distinctively different from that of conventional ZSM-5. During successive deactivation/reactivation cycles, conventional ZSM-5 showed a near-constant reaction rate and an increasing deactivation rate, while hierarchical ZSM-5 showed the opposite behaviors (a decreased reaction rate but a constant deactivation rate). Aramburo et al.[12] reported that mesoporous ZSM-5 prepared by steaming treatment exhibited similar activity and selectivity but better stability in MTH than did untreated ZSM-5 and that different coke species formed in the two catalysts. Ryoo et al.[44] synthesized ZSM-5 nanosheets with only one unit cell thickness that exhibited a 5-fold longer lifetime in comparison to the conventional ZSM-5 catalyst when used for MTH conversion. Most recently, Bhan's group[42] systematically investigated the effect of ZSM-5 crystallite size on product selectivity in MTH conversion. Their results showed that larger crystallites favor the aromatic-based cycle to give higher light-olefin selectivity, because of the prolonged intracrystalline residual time of methylbenzenes. In this study, hierarchically structured (self-pillared) ZSM-5, with a diffusion length as short as ∼1 nm, was used as the representatively smallest crystallite.

Here, we endeavor to explore the influence of mesoporosity in zeolite Beta on its catalytic performance for the MTH reaction by systematically comparing highly mesoporous zeolite Beta (Beta-MS) with conventional zeolite Beta (Beta-C). We analyzed the full products and probed the coke species and their distributions in the catalysts with the assistance of electron microscopy and electron energy loss spectroscopy. The data we obtained explain the difference between the two catalysts and provide important insights into the influence of intracrystalline mesoporosity on the catalytic properties of zeolites.

EXPERIMENTAL SECTION

Preparation of the Catalysts. Beta-MS was hydrothermally synthesized from an aluminosilicate gel using a cationic polymer (polydiallyldimethylammonium chloride) as a template; a detailed description of its synthesis can be found in our recent publication.[26] Beta-C was synthesized according to a previously reported method.[45] To convert zeolites to the H form, the as-synthesized zeolite was ion-exchanged overnight with a 0.5 M NH_4NO_3 solution (20 mL per gram of zeolite) three times, dried in air at 70 °C, and then calcined at 550 °C in air for 4 h.

Characterizations of the Catalysts. Scanning transmission electron microscopy (STEM) images were acquired on a FEI Titan ST Microscope operated at 300 kV using a high-angle annular dark field (HAADF) detector. High-resolution TEM was performed on a JEOL JEM-3010 TEM at 300 kV. Inductively coupled plasma-optical emission spectroscopy (ICP-OES) was conducted on a Varian 720-ES spectrometer, and the powder X-ray diffraction (XRD) patterns were recorded on a Bruker D8 Advance diffractometer using Cu Kα radiation. Ar adsorption−desorption isotherms were measured on a Micromeritics ASAP 2420 apparatus at 87 K. Thermogravimetric analysis (TGA) was performed on a Netzsch TG 209 F1 machine as the temperature increased

DOI: 10.1021/acscatal.5b01350
ACS Catal. 2015, 5, 5837−5845

from 150 to 850 °C under flowing air at a rate of 25 mL/min and a constant ramping rate of 10 K/min. Temperature-programed desorption (TPD) measurements using NH_3 as the probe molecule were performed on a Micromeritics AutoChem II 2950 apparatus. Before measurements, 0.15 g of the sample was pretreated in He gas (25 mL/min) for 1 h at 500 °C and then cooled to 100 °C. Next, the sample was exposed to a mixed gas (10 mol % NH_3 and 90 mol % He) flow of 20 mL/min for 1 h to ensure the sufficient adsorption of NH_3. Prior to desorption, the sample was flushed in He gas for 3 h. Subsequently, NH_3 desorption was performed in the range of 100−600 °C at a heating rate of 10 °C/min under a He flow of 20 mL/min. In situ Fourier transform infrared spectroscopy (FTIR) spectra of pyridine adsorbed were recorded on a Nicolet iS10 FTIR spectrometer, operating in the transmission mode. The samples were pretreated at 450 °C under a vacuum for 8 h before adsorbing pyridine at room temperature. Before the spectrum was collected, desorption of pyridine was performed at the desired temperatures for 2 h. Magic-angle spinning (MAS) ^{27}Al single-pulse nuclear magnetic resonance (NMR) spectra were recorded on a Bruker Advance 900 WB NMR spectrometer operating at a magnetic field of 21.1 T. The hydrated samples were packed into a 3.2 mm ZrO_2 rotor. Spectra were recorded at a resonance frequency of 234.56 MHz, a spinning rate of 20 kHz, a pulse length of 2.0 μs, and a recycle delay of 1 s for 5000 scans. The chemical shift is referenced to an external standard of $Al(CI)_3{\cdot}6H_2O$ (δ 0 ppm).

Catalytic Reactions. MTH conversion was performed in a stainless steel fixed-bed reactor (i.d. 11 mm) packed with 0.5 g of zeolite catalyst. The catalyst bed was activated in a pure air flow (50 mL/min) at 550 °C for 60 min prior to each run, after which the temperature was decreased to 330 °C, and the air flow was switched to an N_2 (50 mL/min) gas flow mixed with 0.01 mL/min of methanol using a HPLC pump. The desired methanol conversions were achieved by adjusting the w8 hly space velocity (WHSV) in the range of 0.94−12 $g_{MeOH}\ g_{Cat}^{-1}\ h^{-1}$. The reactions were all performed under atmospheric pressure, and the product was analyzed using online gas chromatography. The composition of the effluent was determined by gas chromatography (GC) with a flame ionization detector equipped with Agilent HP-PLOT/Q column (30 m × 0.53 mm × 40 μm). The following temperature programming was applied: 6 °C/min from 50 °C (5 min at the initial temperature) to 230 °C (20 min at the final temperature). The liquid products (C_{6+}) were also collected using an ice bath and then analyzed by a HP-5 column with the following temperature programming: 5 °C/min from 40 °C (1 min at the initial temperature) to 140 °C, and then 10 °C/min to 280 °C (1 min at the final temperature). The results showed that there was only a trace amount (<2%) of C_{8+} aliphatics in the liquid products, which are therefore ignored in the discussion. Dimethyl ether was not considered as a product for the calculation.

Analysis of the Residual Organic Species in Used Catalysts. Residual soluble organic species from catalysts were extracted following a commonly used procedure.[46−48] Specifically, the catalyst was taken out of the reactor after the desired reaction time, and 200 mg of this used catalyst was transferred to a capped Teflon vial and dissolved in 6 mL of 24% HF for 3 h. Then, 6.0 mL of CH_2Cl_2 was added to the solution to extract the liberated organic species from the water phase. After 3 h, the organic phase was separated from the mixture and analyzed using GC and GC-MS equipped with the same HP-5 column (30 m × 0.32 mm × 0.25 μm).

Elemental Carbon Mapping and EELS Spectroscopy. The focused ion beam (FIB) technique was used to cut a thin slice from a deactivated catalyst crystal for carbon mapping and electron energy loss spectroscopy (EELS). FIB sample preparation was conducted on an FEI Helios NanoLab 400S FIB/SEM dual-beam system. Before cross sectioning by FIB and the ion milling process, crystals were presputtered by a thin gold layer with a thickness of 5−10 nm. This layer acted as both a marker and a separator between the coke species inside the crystal, and the Pt/C layer outside the catalyst crystal that was deposited prior to FIB cross sectioning served to protect the sample from being damaged by the ion beam. This step is essential to identify the intrinsic distribution of coke species throughout the cross-section specimen of zeolites and to avoid surface damage by the ion beam and the diffusion of deposited carbonaceous species into the specimen. STEM imaging and EELS were performed on a cubed Titan G2 electron microscope with a probe corrector operated at 300 kV. A Cs-corrected and monochromated STEM probe was used for site-specific characterization of the coke species in zeolites, as it offers both high-spatial (<1.4 Å) and high-energy resolution (~0.2 eV).

RESULTS AND DISCUSSION

The two catalysts investigated in this study, hierarchically structured mesoporous zeolite Beta (denoted Beta-MS) and conventional zeolite Beta (denoted Beta-C), have comparable particle sizes (300−500 and 400−600 nm for Beta-MS and Beta-C, respectively) and are both phase pure, as shown by STEM and XRD (Figure 1a−c). Analysis of the XRD shows that the peaks of Beta-MS are broadened relative to those of Beta-C, suggesting smaller crystallite sizes of the former (Figure 1c). STEM images of higher magnification clearly indicate that unlike Beta-C, which consists of dense crystals, Beta-MS contains crystals with hierarchical structures and remarkable

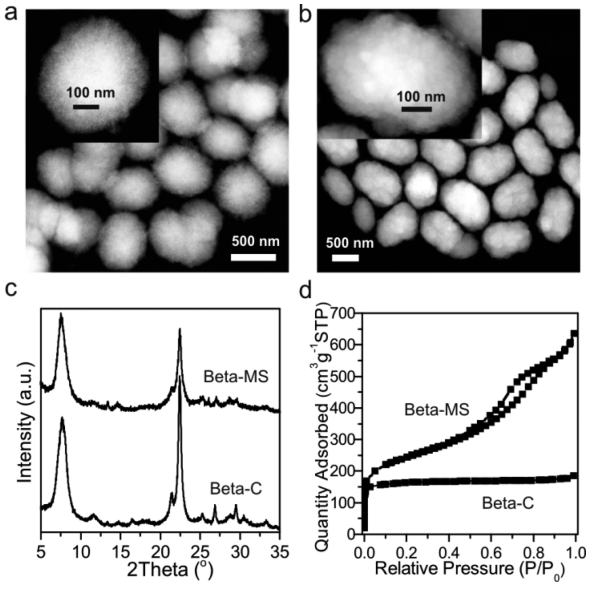

Figure 1. (a, b) STEM images of (a) Beta-MS and (b) Beta-C. (c) XRD patterns of Beta-MS and Beta-C. (d) Ar adsorption−desorption isotherms of Beta-MS and Beta-C collected at 87K. The insets in parts a and b are enlarged STEM images for individual crystals.

DOI: 10.1021/acscatal.5b01350
ACS Catal. 2015, 5, 5837−5845

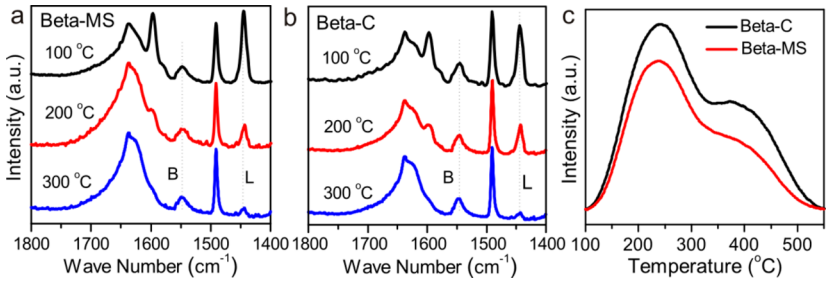

Figure 2. (a, b) FTIR spectra of the characteristic ring vibrations of pyridine adsorbed on Brønsted (B) and Lewis (L) acid sites over Beta-MS (a) and Beta-C (b) catalysts upon desorption treatment at different temperatures. (c) NH_3-TPD profiles of Beta-MS and Beta-C.

intracrystal mesoporosity (insets in Figures 1a,b and Figure S1 in the Supporting Information). This difference is confirmed by the Ar sorption isotherms collected at 87 K. Beta-C exhibits a type I isotherm characteristic of a microporous zeolite, while Beta-MS shows an isotherm with combined type I and type IV isotherm features, indicating the coexistence of micropores and mesopores (Figure 1d). Beta-MS has a slightly larger BET surface area (686 m^2/g vs 623 m^2/g) and a significantly higher total pore volume (0.84 cm^3/g vs 0.27 cm^3/g) than Beta-C. The mesopores in Beta-MS have a relatively narrow size distribution centered at about 8.5 nm, as determined from the adsorption isotherm using the Barrett–Joyner–Halenda model (Figure S2 in the Supporting Information). High-resolution TEM images of Beta-MS show the existence of disordered mesopores that break the microporous zeolite framework into very small but continuous domains, where the smallest crystalline domain is about 3 nm thick (Figure S3 in the Supporting Information). This means that Beta-MS has diffusion lengths of only a few nanometers, 2 orders of magnitude smaller than those of Beta-C. A more detailed structural characterization of Beta-MS, including its single-crystalline nature and three-dimensional interconnection of the mesopores, can be found in our recent publication.[28] Despite the same Si/Al ratio (21) in the synthetic precursors, as-synthesized Beta-MS and Beta-C have slightly different Si/Al ratios (18 and 15, respectively), as determined by ICP-OES. Pyridine adsorption/desorption experiments monitored by FTIR spectra revealed nearly identical Brønsted acidity in the two catalysts (Figure 2a,b). The results of the temperature-programed desorption of ammonia experiments show that Beta-MS has slightly fewer acid sites in comparison to Beta-C (Figure 2c), possibly due to its lower Al content.

The locations of tetrahedrally coordinated Al sites (Al T sites) in the zeolite lattice determine their stability and accessibility and affect the acidity of the zeolite.[49−51] It is interesting to explore whether the fabrication of a hierarchical structure (i.e., the incorporation of mesopores) can cause Al T site distribution to vary for a given zeolite type. Recently, Vjunov et al. used ultrahigh-field ^{27}Al MAS NMR to probe the distribution of Al among the nine crystallographically distinct T sites in zeolite Beta (T1−T9 sites; see Figure 3), and their analysis was based on the deconvolution of the spectra according to the DFT-predicted ^{27}Al NMR chemical shifts.[52,53]

Using this established method, we probed the Al distribution in Beta-MS and Beta-C. Figure 3 shows the ^{27}Al NMR spectra measured at 900 MHz, where by fitting the experimental spectra using the DFT-calculated NMR chemical shifts[52,53] the relative Al occupancies at different T sites were determined. Results show that Al preferentially occupies the T2 site and disfavors the T4−T6 and T8 sites in both Beta-C and Beta-MS.

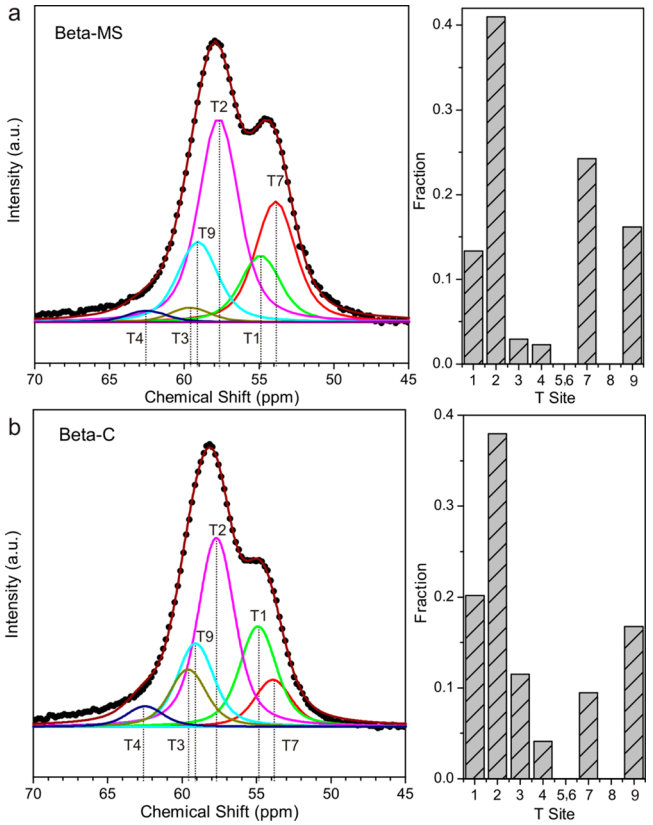

Figure 3. MAS ^{27}Al single-pulse NMR spectra of Beta-MS (a) and Beta-C (b) with the according distribution of different T sites on the right-hand side. The chemical shifts of different T sites used for fitting were adopted from ref 51, which were predicted by DFT calculations. The fitting procedure was similar to that described in ref 51. The black dots and red curves represent the experimental and fitted spectra, respectively. See Figure S4 in the Supporting Information for the nine crystallographic T sites in the zeolite BEA framework.

The major difference between the two samples appears in the fraction of the T7 site, which is considerably higher in Beta-MS (0.25) than in Beta-C (0.09). The T7 site is part of five- and six-membered rings but unassociated with four-membered rings. The observed distribution of Al depends on the occupation probability of Al at each T site as well as the quantity of each T site in the zeolite framework. Assuming that the occupation probabilities are identical for Beta-MS and Beta-C, we conclude that the generation of mesopores (by our direct-synthesis method) results in a large number of surface terminations and, consequently, a change in the relative quantities of different T sites in zeolite Beta. These results indicate that, despite having the same framework type, Beta-MS

DOI: 10.1021/acscatal.5b01350
ACS Catal. 2015, 5, 5837−5845

and Beta-C are substantially different in their distribution of Al T sites. Exploring the subtle influences of this difference on the acid strength of each catalyst is beyond the scope of this study, where we presume that their different catalytic behaviors are mainly associated with their transport properties.

We tested Beta-MS and Beta-C with the MTH reaction using a fixed-bed reactor at 330 °C and 101 KPa total feed pressure. The initial conversion of methanol was controlled by varying the WHSV. Product analysis was performed at steady-state conversions. The details of the reaction conditions and the product analysis methods are elaborated on in the Experimental Section.

First, we investigated the intrinsic selectivity of the catalysts at low conversions. To achieve isoconversion of methanol, a larger WHSV was needed for Beta-MS because of its higher activity in comparison to Beta-C. Specifically, Beta-MS and Beta-C gave ∼20% conversion of methanol (30 min time on stream) at the WHSV of 12 and 5 g_{MeOH} g_{Cat}^{-1} h^{-1}, respectively. Figure 4a shows product selectivity toward ethene,

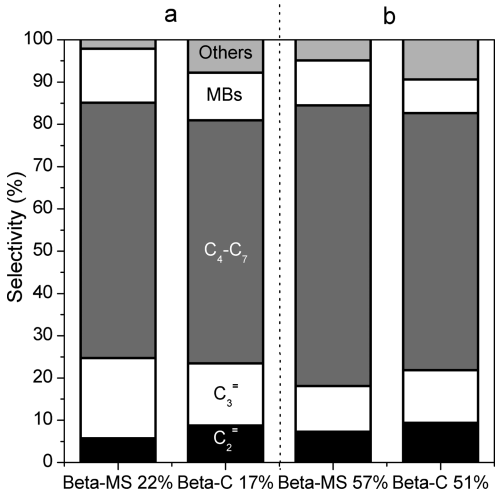

Figure 4. Product selectivity over Beta-MS and Beta-C at two isoconversion (of methanol) conditions: (a) ∼ 20%; (b) ∼ 55%. $C_2^=$, $C_3^=$, C_4−C_7, and MBs stand for ethylene, propylene, C_4−C_7 aliphatics, and methylbenzenes, respectively. The percentages in the horizontal axis specify the exact conversion values given by the corresponding catalyst.

propene, C_4−C_7 aliphatics, methylbenzenes (MBs), and "others" that include ethane, propane, and C_{8+} hydrocarbons, excluding MBs. It is generally accepted that ethene is a termination product of the aromatic-based cycle in MTH. Therefore, ethene selectivity can be used as an indicator for the degree of propagation of this catalytic cycle.[34,39,40] Likewise, higher-hydrocarbon (e.g., C_4−C_7) selectivity is often used to describe the propagation of the olefin-based cycle (Scheme 1).[34,39,40] Note that, because propene can be produced from both cycles and aromatics act as the intermediates of the aromatic-based cycle, their selectivities are not suitable for describing the propagation of the two cycles. Thus, we use the ratio of ethene to C_4−C_7 (ethene/C_4−C_7) yield as a "descriptor" for the relative propagation of the two catalytic cycles. As shown in Figure 4a, Beta-MS produced less ethene but more C_4−C_7 olefins in comparison to Beta-C, giving a smaller ethene/C_4−C_7 yield value (0.095 vs 0.15). Reducing the WHSV to 7 g_{MeOH} g_{Cat}^{-1} h^{-1} for Beta-MS and to 3 g_{MeOH} g_{Cat}^{-1} h^{-1} for Beta-C resulted in the methanol conversion increasing to ∼55%, while Beta-MS still exhibited a lower ethene selectivity, a higher C_4−C_7 selectivity, and accordingly a smaller ethene/C_4−C_7 yield (0.11 vs 0.16) than did Beta-C (Figure 4b). These results suggest that incorporating mesopores in zeolite Beta favors the olefin-based cycle over the aromatic-based cycle. Earlier this year, Bhan's group observed that ethene selectivity decreased while C_4−C_7 hydrocarbon selectivity increased with decreasing crystallite size of the ZSM-5 catalyst. They proposed that the aromatic-based cycle is suppressed by short diffusion lengths because the produced methylbenzene intermediates can easily exit micropores without undergoing further dealkylation reactions that are integral for the aromatic-based cycle which produces ethene.[42] Because our results are in good agreement with these observations, we can infer that although the 12-membered-ring channels of zeolite Beta are sufficiently large for most molecules involved in MTH conversion without restriction, the creation of intracrystalline mesoporosity imposes an impact on the product selectivity similar to that reported for ZSM-5.[42] We note that the effect of crystallite size on the product selectivity is more significant for ZSM-5 than for Beta, likely because ZSM-5 has narrower pores (more severe transport restriction).

We also evaluated the catalytic performance of Beta-MS and Beta-C in terms of conversion capacity, reaction/deactivation rate, selectivity, and lifetime at high conversions of methanol. For this purpose, we adjusted the WHSV to be 0.94 g_{MeOH} g_{Cat}^{-1} h^{-1} for both catalysts to ensure that they handled the same quality of feed. Under this condition, Beta-MS and Beta-C gave 100% and 97% conversions, respectively, at the beginning of the reaction. With prolonged time on stream, conversions of methanol gradually decreased due to catalyst deactivation. Notably, Beta-MS exhibited a significantly slower deactivation rate than Beta-C. As shown in Figure 5, the lifetime before the conversion dropped to 50% was 24.5 h for Beta-MS and 9.0 h for Beta-C.

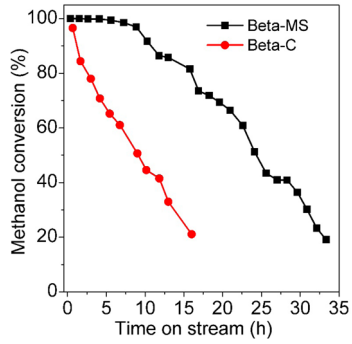

Figure 5. Catalytic lifetime in MTH reactions over Beta-MS and Beta-C catalysts at 330 °C and a WHSV of 0.94 g_{MeOH} g_{Cat}^{-1} h^{-1}.

A model developed by Janssens was used to derive the conversion capacity *R*, the rate constant *k*, and the deactivation coefficient *a* from the lifetime plots.[54] The results clearly show that Beta-MS has a greater conversion capacity *R* (0.72 vs. 0.27 mol_{MeOH} g_{Cat}^{-1}), a higher rate constant *k* (1.2 vs 0.6 mol_{MeOH} g_{Cat}^{-1} h^{-1}), and a lower deactivation coefficient *a* (0.139 vs. 0.378 g_{Cat} mol_{MeOH}^{-1}) in comparison to Beta-C (Table 1). Given that the two catalysts have identical framework types with comparable crystal sizes and Si/Al ratios, the superior catalytic performance of Beta-MS can be attributed to its unique hierarchical structure. The highly interconnected

DOI: 10.1021/acscatal.5b01350
ACS Catal. 2015, 5, 5837−5845

Table 1. Factors of Catalytic Performance Derived from Janssens' Model[a]

catalyst	$t_{0.5}$ (h)[b]	$t_{0.8}$ (h)[c]	R (mol_{MeOH} g_{Cat}^{-1})[d]	k (mol_{MeOH} g_{Cat}^{-1} h^{-1})[e]	a (g_{Cat} mol_{MeOH}^{-1})[f]
Beta-C	9	2.5	0.27	0.6	0.378
Beta-MS	24.5	16	0.72	1.2	0.139

[a]Refer to ref 53 for the details of this model. [b]Time until 50% of conversion. [c]Time until 80% of conversion. [d]Methanol conversion capacity calculated at $t_{0.5}$: $R = WHSV_{MeOH}t_{0.5}$. [e]Rate constant k derived from Janssens' model at $t_{0.8}$. [f]Deactivation coefficient: $a = \tau_0/t_{0.5}$ (contact time: τ_0 = 3.4 g_{cat} h mol_{MeOH}^{-1}).

mesoporous network within Beta-MS crystals allows all acid sites in the catalyst particles to be fully accessible and thus gives a high conversion rate and a large conversion capacity; meanwhile, it reduces the probability of coke formation (by promoting molecular transport) and increases the coke tolerance capacity, which accounts for the long lifetime of the catalyst. In contrast, due to diffusion constraints, the conversion of methanol over Beta-C mainly takes place on the outer layer of catalyst particles where coke is easily accumulated, subsequently blocking reacting molecule access to the interior acid sites and quickly deactivating the catalyst. The insufficient use of active sites explains the inferior catalytic performance of Beta-C in comparison to Beta-MS. We verified these hypotheses by observing the distribution of coke in the deactivated catalysts (vide infra).

We monitored the changes of product selectivity with time on stream until the catalysts were essentially deactivated (conversion <20%). As illustrated in Figure 6a,b, respectively,

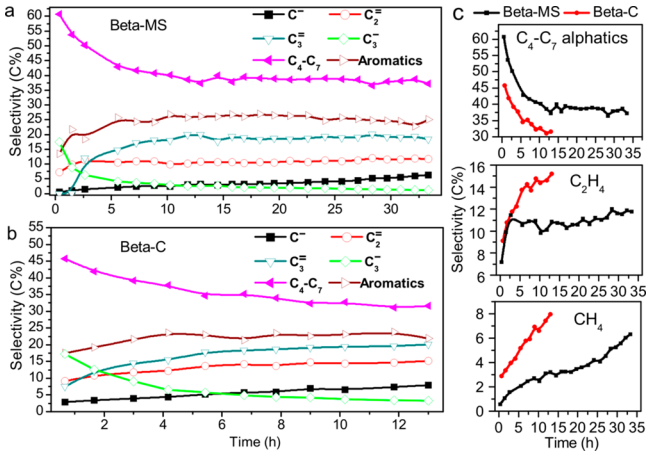

Figure 6. (a, b) Evolution of product selectivity during the MTH conversion reaction over (a) Beta-MS and (b) Beta-C. (c) Isolated selectivities toward C_4−C_7 aliphatics, ethene, and methane shown in parts a and b for direct comparison between the two catalysts.

Beta-MS and Beta-C show similar evolution trends of product selectivity. At the beginning of the reaction, both catalysts gave C_4−C_7 aliphatics as the main products (butene dominating in this fraction), but their selectivity quickly decreased as the reaction proceeded. Propane was the other product with decreased selectivity, while all other identified products, including aromatics, propene, ethene, and methane, showed gradually increased or constant selectivity with prolonged time on stream (Figure 6a,b). These results suggest that, over both catalysts, the olefin-based cycle dominates in the initial stage of the reaction but the aromatic-based cycle is gradually boosted as the reaction proceeds. Meanwhile, certain marked differences in selectivity were evident between the two catalysts. Beta-MS produced more C_4−C_7 aliphatics than Beta-C throughout the whole lifetime: selectivity decreased from 61% to 38% over 30 h for Beta-MS but from 46% to 31% within 12 h for Beta-C (Figure 6c). As the major product of this fraction, butene followed the same trend of selectivity over the two catalysts (Figure S5 in the Supporting Information). Alternatively, over the entire reaction period, Beta-MS had lower ethene selectivity and methane selectivity than Beta-C (Figure 6c). Because ethene and methane are both termination products of the aromatic-based cycle via the dealkylation of MBs,[34,39,40] we can conclude that Beta-MS favors the olefin-based cycle over the aromatic-based cycle, in comparison with Beta-C. These results are consistent with the above discussion about low methanol conversions and can be attributed to the easy molecular transport in Beta-MS that reduces opportunities for MBs to undergo multiple methylation/dealkylation reactions.

Next, we investigated the coke species formed by each catalyst to help further explain their catalytic behaviors. Thermogravimetric analysis of the used catalyst determined the coke content according to weight loss between 300 and 800 °C. Interestingly, despite the fact that it converted more methanol (Figure 5), Beta-MS produced less coke than Beta-C at the same reaction time; for example, after 5 h, coke contents were measured for Beta-MS and Beta-C at 8.7 and 11.7 wt %, respectively (Figure 7a). The slower coke formation in Beta-

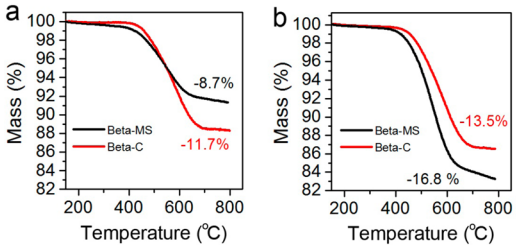

Figure 7. (a) TGA analysis of Beta-MS and Beta-C catalysts after 5 h of reaction. (b) TGA analysis of the completely deactivated Beta-MS and Beta-C catalysts. The weight losses indicated in the figure correspond to the coke contents.

MS can be attributed to its hierarchical structure, which provides better molecular diffusion to depress the polymerization of aromatic hydrocarbons. However, on complete deactivation, more coke accumulated in Beta-MS (16.8 wt %) than in Beta-C (13.5 wt %), indicating that Beta-MS has a higher tolerance capacity to coke (Figure 7b). We used the FIB technique to cut ultrathin cross-section specimens (60−80 nm thick) out of completely deactivated catalyst crystals. From these specimens, we were able to probe the distribution of the coke in the two catalysts using STEM and EELS. Elemental carbon (K-edge) mapping by EELS reveals an obvious difference between the two catalysts: Beta-MS has a fairly uniform coke distribution throughout the entire crystal, while Beta-C exhibits an inhomogeneous distribution of coke that is concentrated at the outer layer and is scarce in the inner region

DOI: 10.1021/acscatal.5b01350
ACS Catal. 2015, 5, 5837−5845

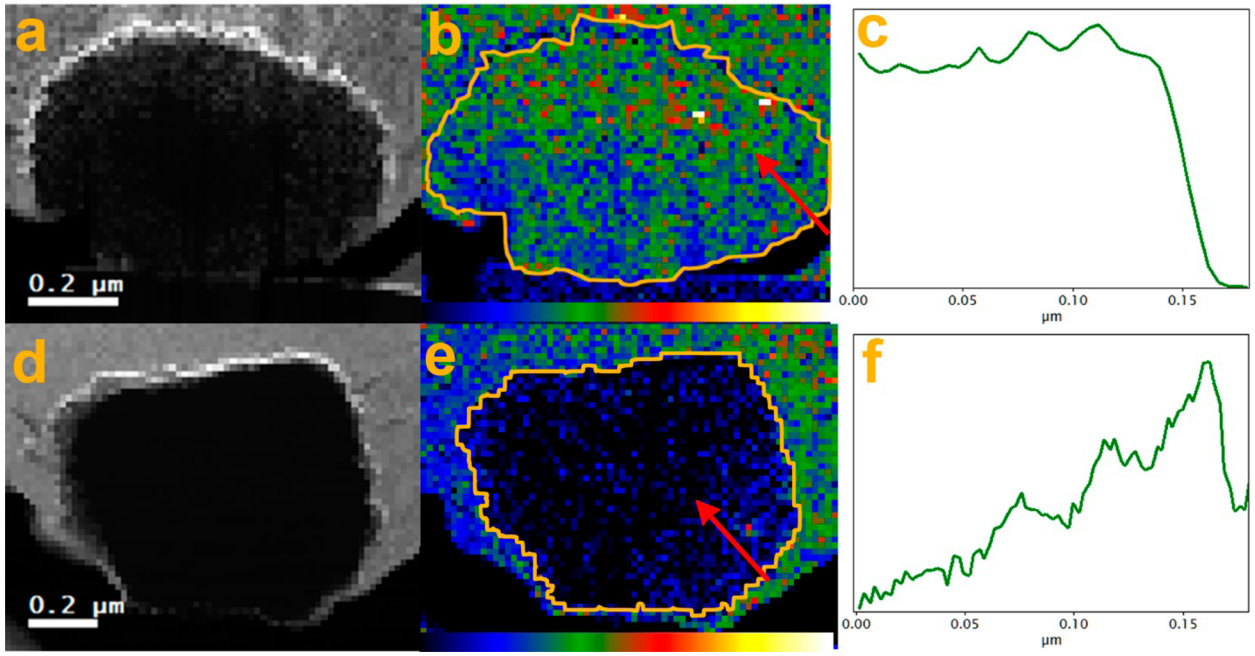

Figure 8. Spectral images, including HAADF-STEM images (left), carbon K-edge intensity maps (middle), and line profiles (right) of Beta-MS (a–c) and Beta-C (d–f). The yellow contour lines in parts b and e mark the Au layers, which show sharp bright contrast in parts a and d. The intensity maps in parts b and e were rendered using a temperature color scheme, as indicated by the color bar. Red arrows indicate where the line profiles were extracted.

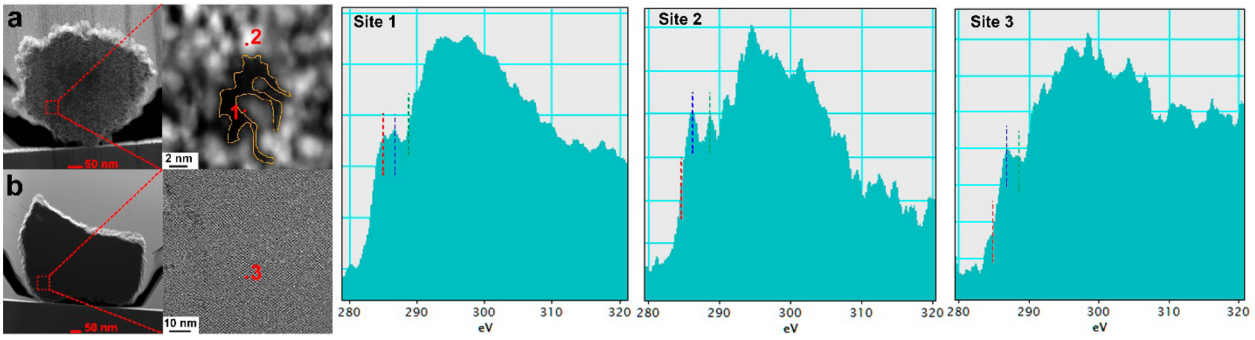

Figure 9. HAADF-STEM images of cross sections of (a) Beta-MS and (b) Beta-C. Local regions are enlarged to show the locations where EELS spectra (on the right) were collected. An irregular mesopore in Beta-MS is outlined in yellow in the zoomed image. Carbon K-edge EELS spectra collected from sites 1–3 are shown on the right, in which different characteristic energy loss peaks are marked by dashed lines with different colors (red, ~285.1 eV; blue, ~286.5 eV; green, ~288.4 eV).

of the crystal (Figure 8). This result is consistent with the TGA analysis showing that Beta-MS can tolerate more coke than Beta-C. More importantly, the result reveals the different reaction sites of the two catalysts. With Beta-C, due to the diffusion restriction imposed by the microporous system, the conversion essentially takes place at the outer surface of catalyst crystals, where once a dense layer of coke is formed the interior acid sites are blocked and become useless for catalysis. In the case of Beta-MS, all acid sites of the catalyst are accessible because the hierarchical structure circumvents the diffusion constraints. This difference explains the greater conversion capacity, the faster reaction rate, and longer lifetime of Beta-MS in comparison to Beta-C.

In addition to the overall distribution of coke, high-resolution EELS (energy resolution of ~0.2 eV along with a small focal depth of <10 nm) allowed us to probe the chemical nature of coke species at specific locations in the catalyst crystals. From two other FIB-cut specimens (the two FIB-cut specimens used for Figure 8 were contaminated after the scanning for carbon mapping), we acquired two EELS spectra for Beta-MS by focusing the electron beam on a mesopore region (site 1) and a zeolite domain (site 2), respectively, and one EELS spectrum for Beta-C (site 3) (see Figure 9). By comparing the EELS fine structures of the three sites, we learn that site 1 has a 1s → π^* excitation at 285.1 eV, which is conventionally assigned to large aromatics with high degrees of graphitization[55,56] and does not appear in the EELS spectra of sites 2 or 3 (Figure 9). Sites 2 and 3 both show a peak of higher energy loss (288.6 eV for site 2 and 288.4 eV for site 3) that is absent from site 1's spectrum. This peak can be attributed to the C–H 1s-3p/σ^* resonance and thus is reasonably considered to be indicative of the existence of H-rich carbon species.[56] These results suggest that, for conventional zeolites, the coke residues in the micropores are low-molecular-weight H-rich species (e.g., MBs and long-chain aliphatics), while heavier graphite-like coke deposits are formed on only the outer surfaces of the catalyst particles. This

DOI: 10.1021/acscatal.5b01350
ACS Catal. 2015, 5, 5837–5845

is conceivable, considering the small dimensions of zeolitic micropores. In the case of Beta-MS, however, the intracrystalline mesopores are sufficiently large to accommodate heavy coke with high degrees of graphitization. More interestingly, we observed another 1s → π^* excitation at ~286.5 eV in the EELS spectra for both Beta-MS and Beta-C (Figure 9), which is a sign of the presence of aromatic C═O sp^2 carbon species in the coke.[56] It was recently proposed that oxygen-containing species may be a possible cause for the deactivation of MTH catalysts, especially in the initial period of the reaction.[57] However, no specific oxygen-containing species have yet been identified, and their formation mechanism remains unclear. Our EELS results provide evidence for the presence of oxygen-containing species in the coke and specifies that they contain aromatic C═O bonds.

To gain more information about the coke, we extracted the organic species retained in the catalysts after different reaction times by using the standard method: dissolution of the zeolite aluminosilicate framework with HF solution followed by extraction of the organic species with CH_2Cl_2 from the water phase.[46−48] The extracted (soluble) species, which are essentially the H-rich compounds residing in the zeolitic micropores and account for ~5 wt % of the total coke, were analyzed with GC and GC-MS. In good agreement with the EELS results, an oxygen-containing compound was identified by GC at a retention time of 26 min as C_8H_8O (m/z 120). On the basis of the fragmentation pattern, the most plausible molecule is 4-methylbenzaldehyde (see Figure 10 and Figures S6 and S7 in the Supporting Information). This compound was detected in the residues of both Beta-MS and Beta-C at different reaction times (Figure 10). 4-Methylbenzaldehyde was only detected in the coke but not in the effluent products of the reaction, suggesting that, once produced, this compound strongly adsorbs on the active sites of zeolite catalysts or is quickly converted into other products (most likely aromatics). It is worth noting that we also identified two oxygen-containing compounds (dimethyl- and trimethyl-2-cyclopenten-1-one) in the coke when zeolite ZSM-5 was used for MTH conversion. A detailed investigation of these unreported coke species, including their content, formation mechanism, and influences on the catalyst activity, will be reported elsewhere shortly.

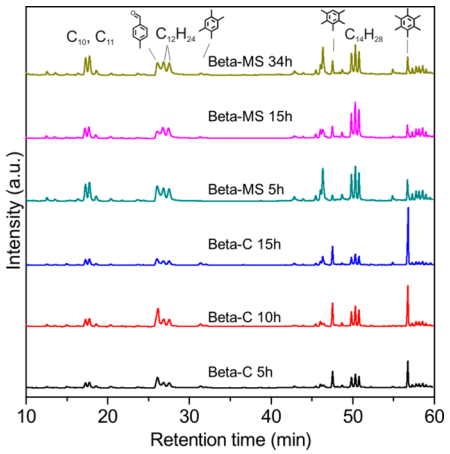

Figure 10. Residual hydrocarbon species extracted from the used catalysts after different reaction times (5, 10, and 15 h for Beta-C; 5, 15, and 34 h for Beta-MS).

With the exception of 4-methylbenzaldehyde, the residual organic species can be classified into MBs (dominated by hexamethylbenzene and pentamethylbenzene) and long-chain aliphatics (C_{10}, C_{11}, C_{12}, C_{14}, etc.). As shown in Figure 10, the relative proportions of MBs and long-chain aliphatics differ greatly between Beta-MS and Beta-C. With an increase in reaction time from 5 to 15 h, the content of MBs in Beta-C gradually accumulated. In comparison, an apparently smaller fraction of MBs remained in Beta-MS, even when the catalyst was nearly completely deactivated (after 34 h of reaction). On the other hand, there was a larger fraction of long-chain aliphatics in Beta-MS than in Beta-C regardless of the reaction time (Figure 10). These results provide additional evidence for our aforementioned conclusions that Beta-MS allows for the easy diffusion of MBs out of the microporous channels due to the hierarchical structure, subsequently suppressing the propagation of the aromatic-based cycle relative to the olefin-based cycle; the opposite effect applies to Beta-C.

CONCLUSIONS

In summary, we systematically compared the catalytic properties between hierarchically porous Beta-MS with conventional microporous Beta-C for MTH conversions. Our results show that the significant intracrystalline mesoporosity is indeed advantageous for improving the accessibility of acid sites in the catalyst crystals, thus giving rise to a larger conversion capacity, a faster conversion rate, and a longer catalyst lifetime. This mesoporosity also enables Beta-MS to afford more coke than Beta-C before complete deactivation. On the other hand, the 2 order of magnitude difference in diffusion length results in different product selectivities between Beta-MS and Beta-C. Methylbenzenes, which are the intermediates of the aromatic-based cycle in the MTH reaction, can easily diffuse out of the zeolite channels in Beta-MS, limiting the propagation of this catalytic cycle, while relatively promoting the olefin-based cycle. As a consequence, Beta-MS gave lower ethene selectivity but higher selectivity toward C_4−C_7 aliphatics with respect to Beta-C in a wide range of methanol conversion (20−100%). We analyzed the residual coke species in the used catalysts and found a smaller ratio of MBs: long-chain aliphatics in Beta-MS in comparison to Beta-C regardless of the reaction time. This result provides further evidence for the suppressed aromatic-based cycle in Beta-MS. Using FIB, STEM, and EELS techniques, we were able to visualize the distribution of coke in the deactivated catalysts. The results verify our hypothesis that all the acid sites in Beta-MS were fully used for catalysis whereas a large fraction of acid sites in Beta-C was blocked (useless for catalysis) by a layer of coke that formed on the crystal's outer surfaces. Results from EELS implied the presence of oxygen-containing compounds in the coke, and accordingly 4-methylbenzaldehyde was identified in the residual organic species by GC-MS. The formation mechanism of such a compound in MTH reactions has had little exposure in the literature, and its role in deactivating the catalyst may be worthy of careful investigations in the future.

ASSOCIATED CONTENT

Supporting Information

The Supporting Information is available free of charge on the ACS Publications website at DOI: 10.1021/acscatal.5b01350.

Additional structures, images, and analytical data (PDF)

DOI: 10.1021/acscatal.5b01350
ACS Catal. 2015, 5, 5837−5845

AUTHOR INFORMATION

Corresponding Author

*E-mail for Y.H.: yu.han@kaust.edu.sa.

Notes

The authors declare no competing financial interest.

ACKNOWLEDGMENTS

This work was supported by the KAUST Office of Competitive Research Funds (OCRF) under Awards No. FCC/1/1972-03-01 and FCC/1/1974-02-01.

REFERENCES

(1) Calero, S.; Schenk, M.; Dubbeldam, D.; Maesen, T. L. M.; Smit, B. *J. Catal.* **2004**, *228*, 121−129.
(2) Jae, J.; Tompsett, G. A.; Foster, A. J.; Hammond, K. D.; Auerbach, S. M.; Lobo, R. F.; Huber, G. W. *J. Catal.* **2011**, *279*, 257−268.
(3) Primo, A.; Garcia, H. *Chem. Soc. Rev.* **2014**, *43*, 7548−7561.
(4) Rownaghi, A. A.; Rezaei, F.; Hedlund, J. *Catal. Commun.* **2011**, *14*, 37−41.
(5) Qin, Z.; Lakiss, L.; Tosheva, L.; Gilson, J.-P.; Vicente, A.; Fernandez, C.; Valtchev, V. *Adv. Funct. Mater.* **2014**, *24*, 257−264.
(6) Zhang, X.; Liu, D.; Xu, D.; Asahina, S.; Cychosz, K. A.; Agrawal, K. V.; Al Wahedi, Y.; Bhan, A.; Al Hashimi, S.; Terasaki, O.; Thommes, M.; Tsapatsis, M. *Science* **2012**, *336*, 1684−1687.
(7) Serrano, D. P.; Escola, J. M.; Pizarro, P. *Chem. Soc. Rev.* **2013**, *42*, 4004−4035.
(8) Chen, L. H.; Li, X. Y.; Rooke, J. C.; Zhang, Y. H.; Yang, X. Y.; Tang, Y.; Xiao, F. S.; Su, B. L. *J. Mater. Chem.* **2012**, *22*, 17381−17403.
(9) Parlett, C. M. A.; Wilson, K.; Lee, A. F. *Chem. Soc. Rev.* **2013**, *42*, 3876−3893.
(10) Perez-Ramirez, J.; Christensen, C. H.; Egeblad, K.; Christensen, C. H.; Groen, J. C. *Chem. Soc. Rev.* **2008**, *37*, 2530−2542.
(11) Holm, M. S.; Taarning, E.; Egeblad, K.; Christensen, C. H. *Catal. Today* **2011**, *168*, 3−16.
(12) Aramburo, L. R.; Teketel, S.; Svelle, S.; Bare, S. R.; Arstad, B.; Zandbergen, H. W.; Olsbye, U.; de Groot, F. M. F.; Weckhuysen, B. M. *J. Catal.* **2013**, *307*, 185−193.
(13) Groen, J. C.; Moulijn, J. A.; Pérez-Ramírez, J. *Microporous Mesoporous Mater.* **2005**, *87*, 153−161.
(14) Ogura, M.; Shinomiya, S.-y.; Tateno, J.; Nara, Y.; Kikuchi, E.; Matsukata, M. *Chem. Lett.* **2000**, *29*, 882−883.
(15) Pérez-Ramírez, J.; Abelló, S.; Bonilla, A.; Groen, J. C. *Adv. Funct. Mater.* **2009**, *19*, 164−172.
(16) Verboekend, D.; Pérez-Ramírez, J. *Chem. - Eur. J.* **2011**, *17*, 1137−1147.
(17) Wang, D. R.; Zhang, L.; Chen, L.; Wu, H. H.; Wu, P. *J. Mater. Chem. A* **2015**, *3*, 3511−3521.
(18) Choi, M.; Cho, H. S.; Srivastava, R.; Venkatesan, C.; Choi, D.-H.; Ryoo, R. *Nat. Mater.* **2006**, *5*, 718−723.
(19) Wang, H.; Pinnavaia, T. J. *Angew. Chem., Int. Ed.* **2006**, *45*, 7603−7606.
(20) Na, K.; Jo, C.; Kim, J.; Cho, K.; Jung, J.; Seo, Y.; Messinger, R. J.; Chmelka, B. F.; Ryoo, R. *Science* **2011**, *333*, 328−332.
(21) Xu, D.; Ma, Y.; Jing, Z.; Han, L.; Singh, B.; Feng, J.; Shen, X.; Cao, F.; Oleynikov, P.; Sun, H.; Terasaki, O.; Che, S. *Nat. Commun.* **2014**, *5*, 4262−4270.
(22) Wang, L.; Zhang, J.; Yi, X.; Zheng, A.; Deng, F.; Chen, C.; Ji, Y.; Liu, F.; Meng, X.; Xiao, F.-S. *ACS Catal.* **2015**, *5*, 2727−2734.
(23) Xi, D.; Sun, Q.; Xu, J.; Cho, M.; Cho, H. S.; Asahina, S.; Li, Y.; Deng, F.; Terasaki, O.; Yu, J. *J. Mater. Chem. A* **2014**, *2*, 17994−18004.
(24) Wang, C.; Yang, M.; Tian, P.; Xu, S.; Yang, Y.; Wang, D.; Yuan, Y.; Liu, Z. *J. Mater. Chem. A* **2015**, *3*, 5608−5616.
(25) Sun, Q.; Wang, N.; Xi, D.; Yang, M.; Yu, J. *Chem. Commun.* **2014**, *50*, 6502−6505.
(26) Kim, J.; Choi, M.; Ryoo, R. *J. Catal.* **2010**, *269*, 219−228.
(27) Mei, C.; Wen, P.; Liu, Z.; Liu, H.; Wang, Y.; Yang, W.; Xie, Z.; Hua, W.; Gao, Z. *J. Catal.* **2008**, *258*, 243−249.
(28) Zhu, J.; Zhu, Y.; Zhu, L.; Rigutto, M.; van der Made, A.; Yang, C.; Pan, S.; Wang, L.; Zhu, L.; Jin, Y.; Sun, Q.; Wu, Q.; Meng, X.; Zhang, D.; Han, Y.; Li, J.; Chu, Y.; Zheng, A.; Qiu, S.; Zheng, X.; Xiao, F. S. *J. Am. Chem. Soc.* **2014**, *136*, 2503−2510.
(29) Olsbye, U.; Svelle, S.; Bjorgen, M.; Beato, P.; Janssens, T. V.; Joensen, F.; Bordiga, S.; Lillerud, K. P. *Angew. Chem., Int. Ed.* **2012**, *51*, 5810−5831.
(30) Dahl, I. M.; Kolboe, S. *J. Catal.* **1994**, *149*, 458−464.
(31) Dahl, I. M.; Kolboe, S. *J. Catal.* **1996**, *161*, 304−309.
(32) Svelle, S.; Joensen, F.; Nerlov, J.; Olsbye, U.; Lillerud, K. P.; Kolboe, S.; Bjorgen, M. *J. Am. Chem. Soc.* **2006**, *128*, 14770−14771.
(33) Bjørgen, M.; Svelle, S.; Joensen, F.; Nerlov, J.; Kolboe, S.; Bonino, F.; Palumbo, L.; Bordiga, S.; Olsbye, U. *J. Catal.* **2007**, *249*, 195−207.
(34) Ilias, S.; Bhan, A. *ACS Catal.* **2013**, *3*, 18−31.
(35) Teketel, S.; Svelle, S.; Lillerud, K.-P.; Olsbye, U. *ChemCatChem* **2009**, *1*, 78−81.
(36) Teketel, S.; Olsbye, U.; Lillerud, K. P.; Beato, P.; Svelle, S. *Microporous Mesoporous Mater.* **2010**, *136*, 33−41.
(37) Hereijgers, B. P. C.; Bleken, F.; Nilsen, M. H.; Svelle, S.; Lillerud, K. P.; Bjorgen, M.; Weckhuysen, B. M.; Olsbye, U. *J. Catal.* **2009**, *264*, 77−87.
(38) Ilias, S.; Bhan, A. *J. Catal.* **2012**, *290*, 186−192.
(39) Sun, X. Y.; Mueller, S.; Liu, Y.; Shi, H.; Haller, G. L.; Sanchez-Sanchez, M.; van Veen, A. C.; Lercher, J. A. *J. Catal.* **2014**, *317*, 185−197.
(40) Sun, X. Y.; Mueller, S.; Shi, H.; Haller, G. L.; Sanchez-Sanchez, M.; van Veen, A. C.; Lercher, J. A. *J. Catal.* **2014**, *314*, 21−31.
(41) Sugimoto, M.; Katsuno, H.; Takatsu, K.; Kawata, N. *Zeolites* **1987**, *7*, 503−507.
(42) Khare, R.; Millar, D.; Bhan, A. *J. Catal.* **2015**, *321*, 23−31.
(43) Schmidt, F.; Hoffmann, C.; Giordanino, F.; Bordiga, S.; Simon, P.; Carrillo-Cabrera, W.; Kaskel, S. *J. Catal.* **2013**, *307*, 238−245.
(44) Choi, M.; Na, K.; Kim, J.; Sakamoto, Y.; Terasaki, O.; Ryoo, R. *Nature* **2009**, *461*, 246−249.
(45) Camblor, M. A.; Pérez-Pariente, J. *Zeolites* **1991**, *11*, 202−210.
(46) Guisnet, M.; Magnoux, P.; Canaff, C. *Stud. Surf. Sci. Catal.* **1986**, *28*, 701−707.
(47) Magnoux, P.; Roger, P.; Canaff, C.; Fouche, V.; Gnep, N. S.; Guisnet, M. *Stud. Surf. Sci. Catal.* **1987**, *34*, 317−330.
(48) Bjørgen, M.; Olsbye, U.; Kolboe, S. *J. Catal.* **2003**, *215*, 30−44.
(49) Perez-Pariente, J. P.; Sanz, J.; Fornes, V.; Corma, A. *J. Catal.* **1990**, *124*, 217−223.
(50) Maier, S. M.; Jentys, A.; Lercher, J. A. *J. Phys. Chem. C* **2011**, *115*, 8005−8013.
(51) Yu, Z.; Zheng, A.; Wang, Q.; Chen, L.; Xu, J.; Amoureux, J. P.; Deng, F. *Angew. Chem., Int. Ed.* **2010**, *49*, 8657−8661.
(52) Vjunov, A.; Fulton, J. L.; Huthwelker, T.; Pin, S.; Mei, D.; Schenter, G. K.; Govind, N.; Camaioni, D. M.; Hu, J. Z.; Lercher, J. A. *J. Am. Chem. Soc.* **2014**, *136*, 8296−8306.
(53) Vjunov, A.; Fulton, J. L.; Huthwelker, T.; Pin, S.; Mei, D.; Schenter, G. K.; Govind, N.; Camaioni, D. M.; Hu, J. Z.; Lercher, J. A. *J. Am. Chem. Soc.* **2015**, *137*, 2409.
(54) Janssens, T. V. W. *J. Catal.* **2009**, *264*, 130−137.
(55) Klein, R. J.; Fischer, D. A.; Lenhart, J. L. *Langmuir* **2008**, *24*, 8187−8197.
(56) Haberstroh, P. R.; Brandes, J. A.; Gélinas, Y.; Dickens, A. F.; Wirick, S.; Cody, G. *Geochim. Cosmochim. Acta* **2006**, *70*, 1483−1494.
(57) Müller, S.; Liu, Y.; Vishnuvarthan, M.; Sun, X.; van Veen, A. C.; Haller, G. L.; Sanchez-Sanchez, M.; Lercher, J. A. *J. Catal.* **2015**, *325*, 48−59.

DOI: 10.1021/acscatal.5b01350
ACS Catal. 2015, 5, 5837−5845